Soil Dynamics and Earthquake Engineering 165 (2023) 107694

Contents lists available at ScienceDirect

Soil Dynamics and Earthquake Engineering

journal homepage: www.elsevier.com/locate/soildyn

Analytical and numerical study of an eccentric continuous cable bracing system with friction slip mechanism

Hanieh Mohammadpour Roshan, Nader Fanaie *

Department of Civil Engineering, K. N. Toosi University of Technology, Tehran, Iran

ARTICLE INFO

Keywords:
Steel moment frame
Cable bracing
Steel pulley
Friction
Lateral resistance
Energy dissipation

ABSTRACT

This study proposes a very simple and low-cost friction mechanism using a pre-stressed cable passing over two fixed pulleys without rotation along with an eccentric continuous cable bracing as a lateral-resistant system for structures subjected to lateral loading such as earthquake. The performance of this mechanism is investigated using analytical solution method and finite element modeling. The purpose of this system is to provide a structure with sufficient stiffness and lateral resistance as well as energy dissipation through frictional slip between the cable and pulleys. The system exhibits two-phase behavior. In case of a small lateral displacement, the system exhibits high stiffness in the linear elastic phase (first phase) and behaves well under normal winds and small earthquakes. In case of large lateral displacement such as a strong earthquake, the system experiences a nonlinear slip phase (second phase) and, accordingly, exhibits a nonlinear behavior with an increase in stiffness and input energy dissipation which protects the structure from displacement. The seismic performance of the proposed system is investigated in terms of three parameters: friction coefficient, initial pre-stressing force, and span length. As the friction coefficient value increases, the lateral resistance of the system rises. In the event of extra rotation of the cable around the pulleys, the coefficient values at static and dynamic friction phases are 5.6 and 5.1 times those in the frictional state, respectively. The rise of the span length and reduction of initial pre-stressing force decrease the system lateral resistance and the initial stiffness of the system, respectively. Upon increasing the initial pre-stressing force up to twice that of the base state, the slip threshold of the system lateral resistance force increases by 33% and as a result, the system remains more at the static friction phase. Also, by reducing the initial pre-stressing to half of its value in the base state, the lateral resistance force corresponding to the slip threshold of system is decreased by 52%; therefore, the slip of the cable on pulleys is initiated earlier. Finally, the cyclic behavior of the steel moment frame with the proposed system is investigated with ATC24 protocol, which increases the stiffness and energy dissipation by 19% compared to the moment frame without the proposed system.

1. Introduction

Steel moment frames in seismic zones are usually designed such that they can have good ductility. However, unexpected events such as severe earthquakes may cause large floor displacement. Cables are characterized by small cross-sectional area, low weight, and high tensile strength and stiffness. Therefore, the application of cable brace can increase the floor stiffness and strength, which leads to its frequent usage in construction [1]. For this purpose, Hou and Tagawa [2,3] proposed a new bracing method for seismic retrofitting and restricting lateral displacement of steel moment frames using cable and hollow cylinders. Fanaie et al. [4-8] investigated the behavior of cylindrical cable braces and the effects of cylinder rigidity, cable pre-stressing, and rigid cylinder dimensions on cylindrical cable bracing systems. The rigidity of the cylinder was considered in two states of soft and rigid cylinders. For a cylinder with high stiffness (rigid cylinder), lateral displacement was directly linked to the system stiffness. The pre-stressing force was proportional to the system initial stiffness and as the pre-stressing increased, the cables reached the yield strain at smaller displacements. The dimension of the cylinder is one of the important parameters affecting the behavior of cable cylindrical bracing and should create a fracture along the cable. Furthermore, Zahrai and Mousavi [9] utilized cable

* Corresponding author. K. N. Toosi University of Technology, Civil Engineering Department, No. 1346, Vali-Asr Street, P.O. Box. 15875-4416, 19697, Tehran, Iran.

E-mail address: fanaie@kntu.ac.ir (N. Fanaie).

https://doi.org/10.1016/j.soildyn.2022.107694
Received 19 July 2022; Received in revised form 18 November 2022; Accepted 25 November 2022

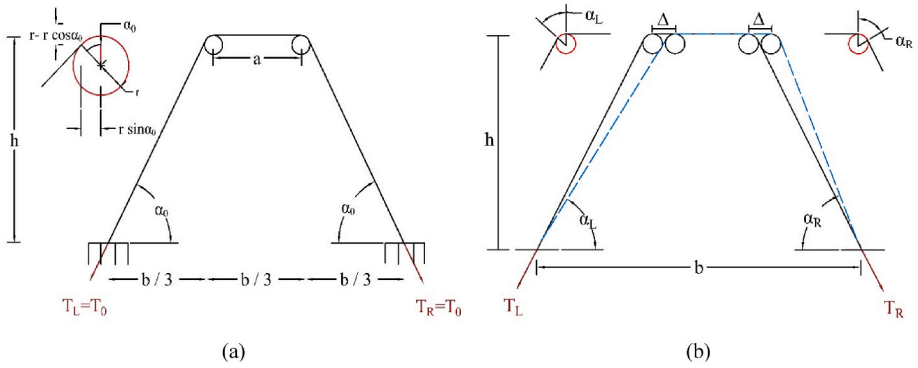

Fig. 1. A view of a continuous eccentric cable bracing system with a new friction damper: (a) Before applying lateral load to the system; (b) After applying lateral load to the system.

with initial loosening to improve the post yield behavior of non-deformable frames with large span. Mehrabi et al. [10] used cable to increase and distribute the lateral stiffness of different floors optimally in an X-cable bracing system with a pre-compressed spring to prevent floor displacement during seismic events.

Ductility and energy dissipation capacity are low despite the high stiffness and strength of steel cables. To this end, in case they are used as braces in structures with the possibility of severe lateral excitations like earthquakes, input energy dissipation occurs in structural components and connections or in energy-dissipation devices (such as dampers) that are added to the system. For this purpose, researchers have used a combination of cable braces and dampers.

At the end of the twentieth century, the applications of energy-dissipation systems grew significantly and led to the development of earthquake excitation response control. Passive energy dissipative devices with low construction and maintenance costs as well as independence from external source by absorbing earthquake input energy have improved the seismic response of structures and these qualities justify their extensive usage [11-18]. Passive dampers including viscous, viscoelastic, metal, mass, and friction dampers have a simple, effective and predefined fixed capacity and their compatibility with a wide range of frequency excitations is limited.

The friction-based damper is the most common and widely used passive energy-dissipation device, which was introduced by Pall et al. based on car brakes [16-21]. The performance of friction dampers is based on dry friction mechanism and the friction results from the slip between two solid pre-stressed surfaces, which provide a specific energy dissipation capacity and have the ability to create an efficient seismic protection system [22,23]. Moghadam et al. [24], for the first time, investigated the applicability of low-cost computational methods for optimizing the multi-level performance of friction dampers implemented in a diagonal bracing system, which led to the calculation of the best friction damper position. The proposed optimal design solution yields a 98% reduction in computational costs, compared to conventional techniques. Friction dampers are less affected by ambient temperature and vibration rate than other types of dampers, which maintain their performance at a constant level [21,25]. Mualla and Belev [26] applied a combination of friction dampers and Chevron cable braces to distribute the input energy of the earthquake and building protection against severe earthquakes, which reduced the base shear. Monir and Zeynali [18] employed a modified friction damper at the intersection of diagonal cable braces in the square section to improve the seismic behavior of steel structures. This system provides the friction required for energy dissipation through friction pads. In recent years, the use of new dampers with the friction slip mechanism has been considered by researchers. For this purpose, for providing strength and lateral stiffness in structural frames, Bagheri et al. [27] used a very simple friction mechanism the cable brace, in which the energy dissipation capacity is provided by passing the pre-stressed cable over a fixed metal cylinder. Francisco et al. [28] used a cable and pulley system connected in series with a spring damper (fluid viscous) in order to provide a high damping rate and reduce the relative response of the structure. This system was installed in a five-story, one-span frame that was considered in four states: i) the structure without cable, pulley, and damper; ii) the structure with an installed damper in each story; iii) the structure with cable, pulley, and damper; and iv) the structure with cable and pulley without damper. Experimental results demonstrated that the system with cable, pulley, and damper had a nonlinear response, which was the result of the interaction between cable and pulley. In addition, the cable and pulley system without damper had a higher energy dissipation rate than the system with only a spring damper. According to the above result, they found that the spring damper played a secondary role in this system and the main role of energy dissipation was the interaction between the cable and the pulley.

According to the investigations, a very simple and low-cost friction mechanism is applied using a pre-stressed cable passing over two fixed pulleys without rotation along with an eccentric continuous cable bracing to create energy dissipation and provide lateral stiffness. This system becomes cost effective by replacing damper with pulleys and has, therefore, a different configuration from the one adopted by Bagheri et al. is used in order to dissipate energy. Furthermore, based on structural analysis, the relationships between the axial force and the system lateral resistance were obtained and then, verified via finite element method. The pre-stressed cable is implemented continuously in a one-story, three-span frame, which passes over the fixed pulleys at the intersection between the diagonal and horizontal parts and is connected to the lower part of the structure. The friction required for energy dissipation in the proposed system is provided by the contact between the steel cable and the pulleys. The proposed system can be used as a resistant lateral system with energy dissipation in structures under lateral environmental loads. This system exhibits linear behavior with high stiffness in case of small displacement, while it enters the nonlinear phase in case of large displacement and prevents the growing displacement. In this research, the proposed system is investigated in two ways: analytical solution and finite element model. The most important effective parameters are considered to be friction coefficient, initial pre-stressing force, and span length. Finally, the moment frame is compared to the one equipped with the proposed system.

2. The analytical solution of the proposed system

The applied cable in the system is pre-stressed with the tension force of $T_0 = EA\varepsilon_0$ where ε_0, E, and A represent pre-stressing strain, Young's modulus, and cross-section, respectively. In Fig. 1 (a), before applying lateral load to the system, the pre-stressed cable with the length of L and the contact angle of $\beta_0 = 2\alpha_0$ is wrapped around the pulleys and the parameters α_0 and L are obtained by the figure geometry.

$$\tan\alpha_0 = \frac{h - r(1 - cos\,\alpha_0)}{\frac{b}{3} - rsin\alpha_0} \tag{1}$$

$$L = 2\sqrt{[hr(1-\cos\alpha_0)]^2 + \left(\frac{b}{3} - r\sin\alpha_0\right)^2} + 2r\alpha_0 + \frac{b}{3} \tag{2}$$

By considering r/h ≪1, Eqs. (3) and (4) can be written by dividing the numerator and denominator of Eq. (1) fraction by h and the simplified form is given below.

$$\tan\alpha_0 = \frac{\frac{h}{h} - \frac{r}{h}(1-\cos\alpha_0)}{\frac{b}{3h} - \frac{r}{h}\sin\alpha_0} = \frac{1}{b/3h} = \frac{3h}{b} \tag{3}$$

$$\mathrm{L} = \frac{\mathrm{b}}{3} + 2\sqrt{\mathrm{h}^2 + \left(\frac{\mathrm{b}}{3}\right)^2} \tag{4}$$

In order to simply solve equations, a dimensionless geometric parameter is defined as Eq. (5), which simplifies the values of α_0 and L as Eqs. (6) and (7).

$$d = \frac{\frac{b}{3}}{h} = \frac{b}{3h} \tag{5}$$

$$\alpha_0 = tan^{-1}\left(\frac{1}{d}\right) \tag{6}$$

$$\mathrm{L} = \frac{b}{3} + 2\sqrt{h^2\left(1 + \left(\frac{b}{3h}\right)^2\right)} = \mathrm{h}\left[\mathrm{d} + 2\sqrt{1+d^2}\right] \tag{7}$$

The pulleys are displaced horizontally by Δ lateral loading, and their vertical displacement and rotation are restricted. Throughout this research, the value of Δ to the right is considered positive. In order to simply solve equations, a dimensionless parameter is defined for the normalized displacement of the pulleys.

$$\delta = \frac{\Delta}{h} \tag{8}$$

According to the modified figure of the system (Fig. 1(b)), the contact angle between the pre-stressed cable and the pulleys is equal to $\beta = \alpha_L + \alpha_R$, where the values of α_L and α_R are obtained using the figure geometry.

$$\tan\alpha_L = \frac{1 - \frac{r}{h}(1 - cos\,\alpha_l)}{d + \delta - \frac{r}{h}\sin\alpha_l} \rightarrow \alpha_L = \tan^{-1}\left(\frac{1}{d+\delta}\right) \tag{9}$$

$$\tan\alpha_R = \frac{1 - \frac{r}{h}(1 - cos\,\alpha_R)}{d - \delta - \frac{r}{h}sin\,\alpha_R} \rightarrow \alpha_R = \tan^{-1}\left(\frac{1}{d-\delta}\right) \tag{10}$$

Given that the value of Δ is small, $\alpha_L \cong \alpha_R \cong \alpha_0$ can be considered. In the proposed system, the pre-stressed cable with friction coefficient of μ is in contact with the pulleys and the system behavior is investigated in two states, i.e., with and without friction.

2.1. Frictionless state $\mu = 0$

In this state, the total change in cable length is defined as $\Delta L = \ell - L$ and the amount of strain is uniform throughout the cable. In the above equation, parameter ℓ is the cable length after deformation, the value of which is calculated according to Fig. 1(b) in Eq. (11) and the value of L is calculated using Eq. (7).

$$\ell = \frac{b}{3} + h\left[\sqrt{1+(d+\delta)^2} + \sqrt{1+(d-\delta)^2}\right] = h\left[d + \sqrt{1+(d+\delta)^2} + \sqrt{1+(d-\delta)^2}\right] \tag{11}$$

$$\begin{aligned}\Delta L &= \ell - L \\ &= h\left[d + \sqrt{1+(d+\delta)^2} + \sqrt{1+(d-\delta)^2}\right] - \mathrm{h}\left[\mathrm{d} + 2\sqrt{1+d^2}\right] \\ &= h\left[d + \sqrt{1+(d+\delta)^2} + \sqrt{1+(d-\delta)^2} - d - 2\sqrt{1+d^2}\right]\end{aligned} \tag{12}$$

$$\frac{\Delta L}{L} = \frac{h\left[\sqrt{1+(d+\delta)^2} + \sqrt{1+(d-\delta)^2} - 2\sqrt{1+d^2}\right]}{\left[h\left(d + 2\sqrt{1+d^2}\right)\right]} \tag{13}$$

The cable strain is calculated via Eq. (14).

$$\varepsilon = \varepsilon_0 + \frac{\Delta \mathrm{L}}{\mathrm{L}} = \varepsilon_0 + \frac{\sqrt{1+(\mathrm{d}+\delta)^2} + \sqrt{1+(\mathrm{d}-\delta)^2} - 2\sqrt{1+\mathrm{d}^2}}{\mathrm{d} + 2\sqrt{1+\mathrm{d}^2}} \tag{14}$$

According to the non-zero term of Taylor series, the cable strain is calculated using Eq. (15).

$$\varepsilon = \varepsilon_0 + \frac{1}{d\left(1+d^2\right)^{\frac{3}{2}} + 2\left(1+d^2\right)^2}\delta^2 \tag{15}$$

In the frictionless state, the cable tension force is as $T_R = T_L = T = EA\varepsilon$ and its normalized value is calculated with T_0 in Eq. (16).

$$\frac{\mathrm{T}}{\mathrm{T}_0} = 1 + \frac{1}{\boldsymbol{\varepsilon_0}\left(d\left(1+d^2\right)^{\frac{3}{2}} + 2\left(1+d^2\right)^2\right)}\delta^2 \tag{16}$$

2.2. Friction state

The left and right sides of cable length changes are $\Delta L_L = \ell_L - L_L$ and $\Delta L_R = \ell_R - L_R$, respectively, which are calculated using Eqs. (17) - (19).

$$\ell_L = h\sqrt{1+(d+\delta)^2} \tag{17}$$

$$\ell_R = h\sqrt{1+(d-\delta)^2} \tag{18}$$

$$L_L = L_R = \sqrt{(h - r(1-\cos\alpha_0))^2 + \left(\frac{b}{3} - r\sin\alpha_0\right)^2} + r\alpha_0 \tag{19}$$

Similarly, for $\frac{r}{h} \ll 1$, Eq. (19) is simplified as follows:

$$L_L = L_R = \sqrt{h^2 + \left(\frac{b}{3}\right)^2} = h\sqrt{1+d^2} \tag{20}$$

$$\frac{\Delta L_L}{L_L} = \frac{\sqrt{1+(d+\delta)^2} - \sqrt{1+d^2}}{\sqrt{1+d^2}} \tag{21}$$

$$\frac{\Delta L_R}{L_R} = \frac{\sqrt{1+(d-\delta)^2} - \sqrt{1+d^2}}{\sqrt{1+d^2}} \tag{22}$$

According to Eqs. (21) and (22), the strain in the left and right sides of the cable is calculated as follows:

$$\varepsilon_L = \varepsilon_0 + \frac{\Delta L_L}{L_L} = \varepsilon_0 + \frac{\sqrt{1+(d+\delta)^2} - \sqrt{1+d^2}}{\sqrt{1+d^2}} \tag{23}$$

$$\varepsilon_R = \varepsilon_0 + \frac{\Delta L_R}{L_L} = \varepsilon_0 + \frac{\sqrt{1+(d-\delta)^2} - \sqrt{1+d^2}}{\sqrt{1+d^2}} \tag{24}$$

Similarly, in the frictionless state, by using the first non-zero terms of the Taylor expansion, the strain in the left and right sides of the cable is simplified as follows:

$$\varepsilon_L = \varepsilon_0 + \frac{d}{1+d^2}\delta \tag{25}$$

$$\varepsilon_R = \varepsilon_0 - \frac{d}{1+d^2}\delta \tag{26}$$

As a result, using Eqs. (25) and (26), the normalized tension forces in the left and right sides of the cable are calculated, where δ_s is the normalized displacement at the slip threshold of the cable on the pulleys. Throughout the research, the index S is related to the slip threshold of the cable on the pulleys.

$$\frac{T_L}{T_0} = 1 + \frac{d}{\varepsilon_0(1+d^2)}\delta \quad \delta \le \delta_s \tag{27}$$

$$\frac{T_R}{T_0} = 1 - \frac{d}{\varepsilon_0(1+d^2)}\delta \quad \delta \le \delta_S \tag{28}$$

The normalized forces of the left- and right-side cables at the slip threshold are as follows:

$$\frac{T_{Ls}}{T_0} = \frac{\varepsilon_0(1+d^2)}{\varepsilon_0(1+d^2)} + \frac{d}{\varepsilon_0(1+d^2)}\delta s \tag{29}$$

$$\frac{T_{Rs}}{T_0} = \frac{\varepsilon_0(1+d^2)}{\varepsilon_0(1+d^2)} - \frac{d}{\varepsilon_0(1+d^2)}\delta_S \tag{30}$$

By placing Eqs. (29) and (30) in the Euler's formula (Eq. (31)), the normalized displacement of the cable at the slip threshold is calculated as follows:

$$T_{Ls} = T_{Rs}\, e^{\mu\beta_s} \tag{31}$$

$$\delta_s = \frac{\varepsilon_0(1+d^2)}{d}\quad \frac{e^{\mu\beta_s}-1}{e^{\mu\beta_s}+1} \tag{32}$$

The parameter β_s in Eq. (32) is the angle of the inclined cable with the horizontal extension. The values of δ_s and ε_0 are infinitely small; thus, the basic geometry of the system does not differ from the system geometry at the slip threshold and it can be assumed that $\beta_s = \beta_0$. To this end, Eq. (33) is obtained as follows:

$$\delta_s = \frac{\varepsilon_0(1+d^2)}{d}\ \frac{e^{\mu\beta_0}-1}{e^{\mu\beta_0}+1} \tag{33}$$

Assuming that $\delta = \delta_s$, the tension forces of the left- and right-side cables at the slip threshold in Eqs. (29) and (30) are simplified to Eqs. (34) and (35).

$$\frac{T_{Ls}}{T_0} = 1 + \frac{e^{\mu\beta_0}-1}{e^{\mu\beta_0}+1} = \frac{2e^{\mu\beta_0}}{e^{\mu\beta_0}+1} \tag{34}$$

$$\frac{T_{Rs}}{T_0} = 1 - \frac{e^{\mu\beta_0}-1}{e^{\mu\beta_0}+1} = \frac{2}{e^{\mu\beta_0}+1} \tag{35}$$

The Euler's formula (Eq. (31)) is valid in the phase of the cable slip on pulleys ($\delta > \delta_s$).

$$T_L = T_R e^{\mu\beta} \rightarrow T_{Ls} + \acute{T_L} = (T_{Rs} + \acute{T_R})e^{\mu\beta} \tag{36}$$

Parameters $\acute{T_R}$ and $\acute{T_L}$ are the additional tension forces of the cable in the right and left sides in the slip state, respectively, which are calculated as $\acute{T_L} = EA\acute{\varepsilon_L}$ and $\acute{T_R} = EA\acute{\varepsilon_R}$. By placing Eqs. (34) and (35) in Eq. (36), the following equation is obtained.

$$\acute{\varepsilon_L} - \acute{\varepsilon_R}e^{\mu\beta} = \varepsilon_0\frac{2(e^{\mu\beta} - e^{\mu\beta_0})}{e^{\mu\beta_0}+1} \tag{37}$$

It can also be written:

$$\acute{\varepsilon_L}L_L + \acute{\varepsilon_R}L_R = \Delta L - (\Delta L_{ls} + \Delta l_{Rs}) \tag{38}$$

In Eq. (38), the parameters ΔL_{Ls} and ΔL_{Rs} are the left- and right-side cable length changes at the slip threshold and $L_{Ls} = L_{Rs}$ is considered.

Through Eqs. (21) and (22), the above is written as follows:

$$\frac{\Delta L_{Ls}}{L_{Ls}} = \frac{\sqrt{1+(d+\delta_s)^2} - \sqrt{1+d^2}}{\sqrt{1+d^2}} \tag{39}$$

$$\frac{\Delta L_{Rs}}{L_{Rs}} = \frac{\sqrt{1+(d-\delta_s)^2} - \sqrt{1+d^2}}{\sqrt{1+d^2}} \tag{40}$$

$$\frac{\Delta L}{L_{Ls}} = \frac{\sqrt{1+(d+\delta)^2} + \sqrt{1+(d-\delta)^2} - 2\sqrt{1+d^2}}{\sqrt{1+d^2}} \tag{41}$$

By placing Eqs. (39) and (40) in Eq. (38), the sum of the additional left- and right-side cable strains is written as follows:

$$\acute{\varepsilon_L}L_L + \acute{\varepsilon_R}L_R = \Delta L - (\Delta L_{ls} + \Delta l_{Rs}) \rightarrow \acute{\varepsilon_L} + \acute{\varepsilon_R} = \frac{\Delta L}{L_{Ls}} - \frac{\Delta L_{Ls} + \Delta L_{Rs}}{L_{Ls}} = \frac{\sqrt{1+(d+\delta_s)^2} + \sqrt{1+(d-\delta_s)^2} - 2\sqrt{1+d^2}}{\sqrt{1+d^2}} - \frac{\sqrt{1+(d+\delta_s)^2} + \sqrt{1+(d-\delta_s)^2} - 2\sqrt{1+d^2}}{\sqrt{1+d^2}} \tag{42}$$

By the first non-zero term in the Taylor series expansion, the right side of Eq. (42) is simplified as follows:

$$\acute{\varepsilon_L} + \acute{\varepsilon_R} = \frac{1}{(1+d^2)^2}(\delta^2 - \delta_s^2) \tag{43}$$

By solving Eqs. (37) and (43), additional strains of the left and right cables are obtained; accordingly, the normalized tension forces by T_0 of the left- and right-side cables can be calculated as follows:

$$\acute{\varepsilon_L} = \frac{e^{\mu\beta}}{(e^{\mu\beta}+1)(1+d^2)^2}(\delta^2 - \delta_s^2) + \frac{2(e^{\mu\beta} - e^{\mu\beta_0})}{(e^{\mu\beta}+1)(e^{\mu\beta_0}+1)}\varepsilon_0 \tag{44}$$

$$\acute{\varepsilon_R} = \frac{1}{(e^{\mu\beta}+1)(1+d^2)^2}(\delta^2 - \delta_s^2) - \frac{2(e^{\mu\beta} - e^{\mu\beta_0})}{(e^{\mu\beta}+1)(e^{\mu\beta_0}+1)}\varepsilon_0 \tag{45}$$

$$\frac{T_L}{T_0} = \frac{T_{Ls}}{T_0} + \frac{\acute{T_L}}{T_0} \rightarrow \frac{T_L}{T_0} = \frac{2e^{\mu\beta_0}}{e^{\mu\beta_0}+1} + \frac{e^{\mu\beta}}{\varepsilon_0(e^{\mu\beta}+1)(1+d^2)^2}(\delta^2 - \delta_s^2) + \frac{2(e^{\mu\beta} - e^{\mu\beta_0})}{(e^{\mu\beta}+1)(e^{\mu\beta_0}+1)} \tag{46}$$

$$\frac{T_R}{T_0} = \frac{T_{Rs}}{T_0} + \frac{\acute{T_R}}{T_0} \rightarrow \frac{T_R}{T_0} = \frac{2}{e^{\mu\beta_0}+1} + \frac{1}{\varepsilon_0(e^{\mu\beta}+1)(1+d^2)^2}(\delta^2 - \delta_s^2) - \frac{2(e^{\mu\beta} - e^{\mu\beta_0})}{(e^{\mu\beta}+1)(e^{\mu\beta_0}+1)} \tag{47}$$

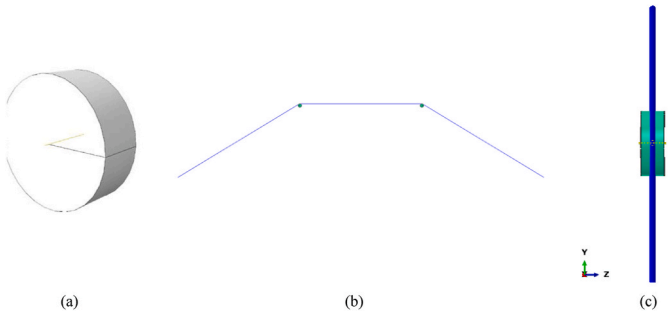

Fig. 2. Model of the proposed system components in Abaqus software: (a) Pulley; (b) Cable bracing system and pulleys, (c) Magnification of the cable and pulleys connection.

The contribution of the last term in Eqs. (46) and (47) is negligible compared to the second term, because the value of ε_0 at the denominator of the second term is infinitely small. In addition, these equations are function of β, which are given in terms of δ normal displacement. Therefore, by using this expansion and ignoring the last terms in Eqs. (46) and (47), these equations can be simplified as follows:

$$\frac{T_L}{T_0} = \frac{2e^{\mu\beta_0}}{e^{\mu\beta_0}+1}\left[1+\frac{1}{2\varepsilon_0\left(1+d^2\right)^2}\left(\delta^2-{\delta_s}^2\right)\right] \quad \delta > \delta_s \tag{48}$$

$$\frac{T_R}{T_0} = \frac{2}{e^{\mu\beta_0}+1}\left[1+\frac{1}{2\varepsilon_0\left(1+d^2\right)^2}\left(\delta^2-{\delta_s}^2\right)\right] \quad \delta > \delta_s \tag{49}$$

Eqs. (27) and (28) together with Eqs. (48) and (49) show the system response, as depicted in Fig. 1.

3. Friction slip mechanism of the proposed system, finite element model and its verification

In the proposed system mechanism, fixed and non-rotating pulleys are welded inside the column at the upper level of the structure and the cable passes over the pulleys and under the beam. Lateral excitements such as earthquakes and wind cause a drift between the upper and lower levels of the structure and this bracing system results in the reduction of the displacement of top of the columns significantly compared to the state without a cable; in other words, system lateral stiffness increases. The input energy is dissipated due to the friction force and friction in this system is provided by the contact between the cable and pulleys.

The friction coefficient between the cable and pulley remains constant in the life time of structure if the proper maintenance can prevent the cable and pulley from corrosion. Whenever an earthquake occurs, heat is generated by the cable slip over the pulley and some of the earthquake input energy is dissipated. This cable bracing system works as a passive control system and since it does not require any special equipment, this bracing system is low-cost and affordable. In addition, another advantage of this system is that it acts like a conventional bracing against wind and small earthquakes and prevents the frame from displacement under lateral loading.

Proven equations in the analytical solution section are validated using the applied model in finite element model in Abaqus software [29]. The pulleys with the radius and thickness of 7 and 5 cm, respectively, are modeled by 'Analytical rigid' method and the deformation of the pulleys is ignored in the modeling'. The cable is modeled as an elastic high-strength steel with Young's modulus of E = 185 GPa, Poisson's ratio of $\nu = 0.3$, and density of $= 7850\,\frac{kg}{m^3}$ in the form of a 1 cm diameter circular cross-section. Fig. 2(b) shows the proposed cable system with pulleys. In the proposed system, the cable only works in tension; thus, the 'No Compression' option is activated and the system is not capable of compression. The constructed model is analyzed using the 'static general' method and the 'Nlgeom' option is enabled to consider nonlinear geometric analysis. The cable is pre-stressed by applying displacement and is meshed with T3D2 truss elements with a maximum element size of 10 mm. The interaction between the cable and pulleys is defined by friction through penalty method and of the 'Hard Contact' type, in which the cable is selected as the slave surface and the pulleys as the master surface.

The boundary condition of the model is as follows: By applying the boundary condition to the center of the pulleys, vertical displacement and rotation of them are restricted and they are only allowed to have horizontal displacement. Both cable ends are restricted by a hinged support to prevent displacement in the horizontal and vertical directions of the cable.

The proposed system is implemented in a three-span frame in which the horizontal part of the cable in the middle span and the two diagonal parts of the cable are on two side spans.

In this study, lateral displacement is applied to the structure from the left span and causes displacement to the right side of the system. In accordance with this assumption, the system is validated and all outputs are extracted and analyzed. The parameters used for validation are a = 5 m, h = 3 m, $d_{cable} = 0.01$, $r_{clinderical} = 0.07$, and E = 185 GPa.

3.1. Verification of cable and pulley bracing system

In order to verify the proven equations, the axial force diagram of the left- and right-side cables is compared to the diagram obtained from finite element model. The axial force diagram of left- and right-side cables in the frictionless state is taken from Eq. (16). In the frictional state with a friction coefficient of 0.3, the left-side cable axial force is drawn by Eqs. (27) and (48) while the right cable axial force is drawn by Eqs. (28) and (49) in Fig. 3. Fig. 3 compares the diagrams of analytical method and finite element and as shown in the figure, the diagrams have an acceptable correlation with each other. According to the figure, the system has a nonlinear phase in the frictionless state, and by imposing friction, the system has two phases of static and dynamic friction, which

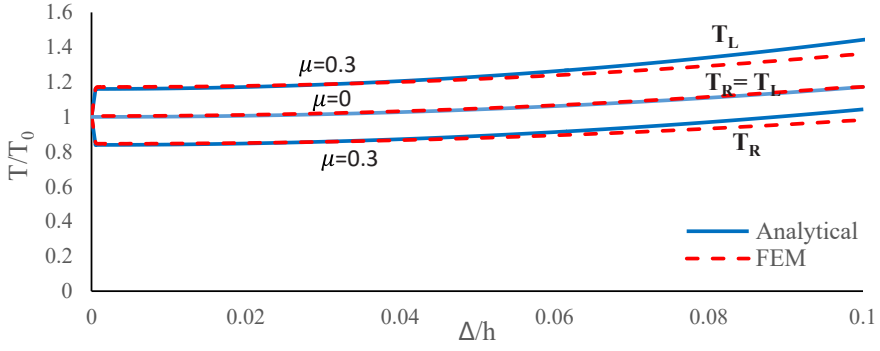

Fig. 3. Verification diagram of the model in Abaqus and the analytical solution with the assumption of $T_0 = 20.76$ kN and a = 5.

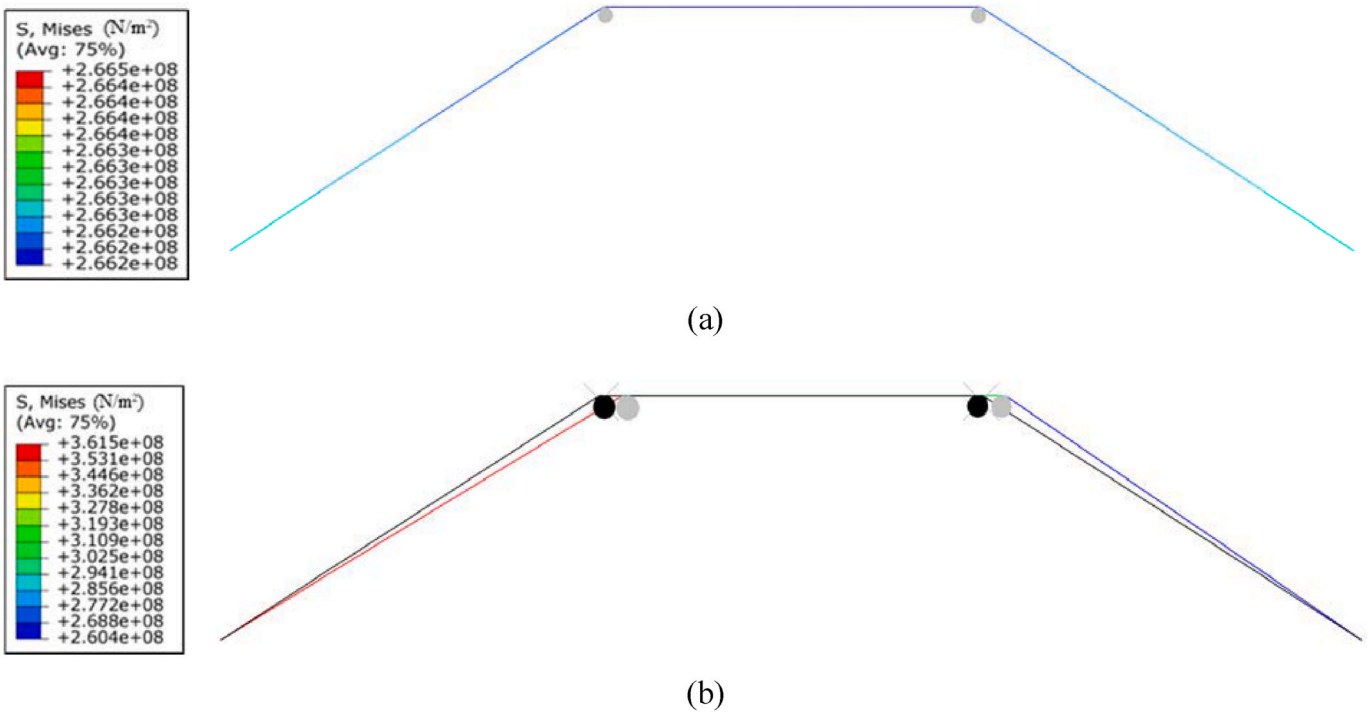

Fig. 4. The proposed system; (a) Shape of the cable and pulley in the state of pre-stressed cables; (b) Final shape of the proposed system after processing.

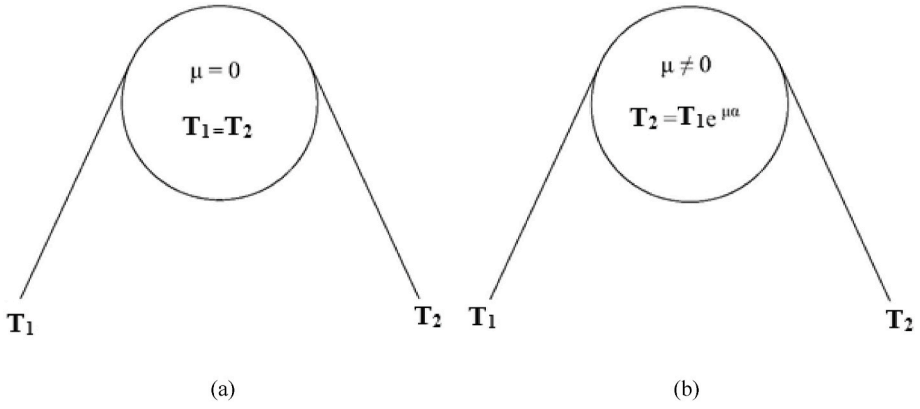

Fig. 5. Static investigation of the cable and the pulley in (a) Frictionless state; (b) Frictional state.

is the system main feature. The system is in a static phase with high stiffness up to the cable slip over the pulleys and after the cable slip over the pulleys, the system stiffness suddenly decreases and enters the dynamic friction phase and prevents system large displacement. Upon the application of lateral displacement to the right, the pulleys have displacement to the right and the tension starts from the left side of the cable and enters the horizontal part of the cable. At the end, the diagonal right-side cable is in tension, which shows the cable permanent tension in the proposed system. Fig. 4(a) shows a view of an eccentric continuous cable bracing system with a new frictional damper after processing in which the cable is pre-stressed and, then, a displacement is applied to pulleys. Fig. 4(b) shows displaced pulleys after system processing.

3.2. Limitations of the cable and pulley bracing system

Before the slip, static friction is considered for the object displacement from the static state and after the slip, the displacement is accompanied by dynamic friction. In two states of static and dynamic friction, the value of the friction coefficient is different so that in case of the same material for both surfaces, the dynamic friction coefficient is lower than the static friction coefficient. One of this research limitations is the assumption of static and dynamic friction coefficients being the same, and their value is assumed to be 0.3 for the base friction coefficient. Another limitation of the proposed system is that the pulleys' rotational degree of freedom is zero and no rotation is allowed during the analysis. In this research, the effect of the initial pre-stressing force of the cable is investigated, while the cable relaxation has not been investigated.

4. Investigating the behavior of the proposed system against lateral load

The proposed system consists of a pre-stressed cable and two pulleys that make frictional contact with them at the point where the cable passes over the pulleys, causing energy dissipation and creating lateral resistant force according to Eq. (50) against the lateral load applied to the system. In the proposed system, three main parameters namely friction coefficient, initial pre-stressing force, and span length are

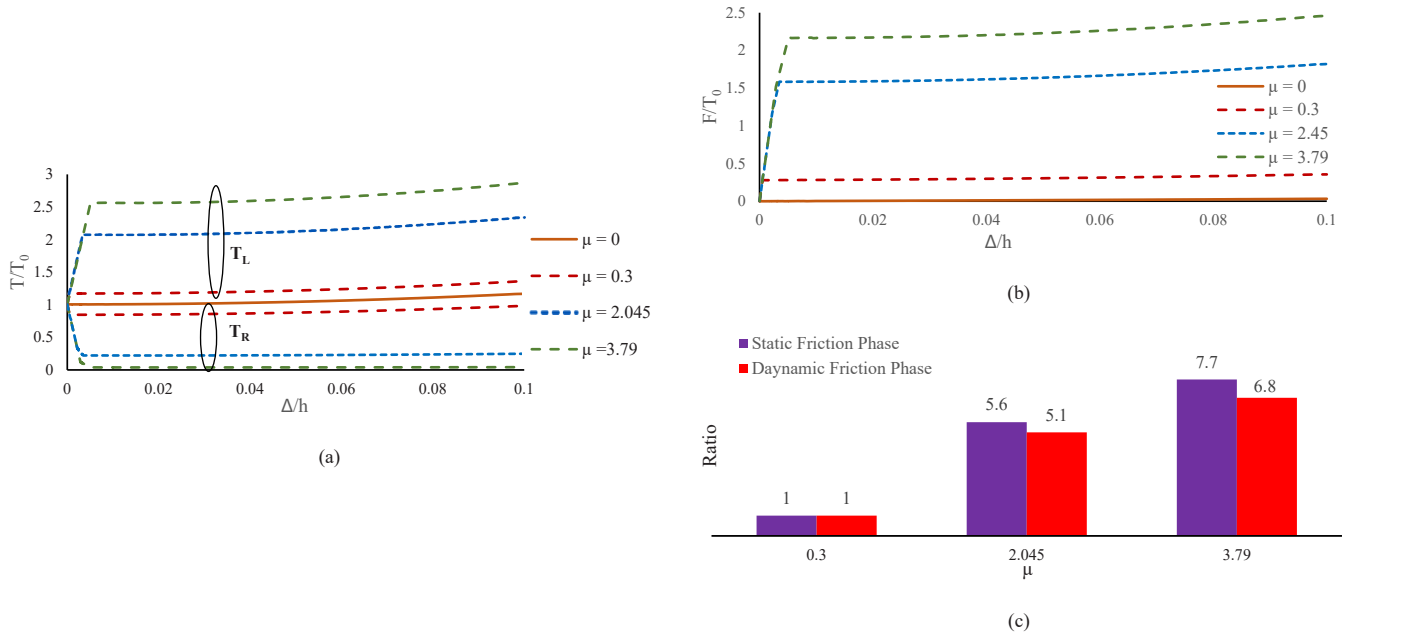

Fig. 6. (a) Normalized axial force diagram; (b) Normalized lateral resistance; (c) Ratio of lateral resistance changes with different friction coefficients.

investigated.

To study the effect of friction coefficient, extra rotation of the cable around the pulleys is used, which increases the contact angle between the cable and pulleys and, thus, increases the friction coefficient. In the case of static cables, if a cable passes over a pulley without friction and the cable is under a tension force, as shown in Fig. 5(a), the cable force is necessarily equal on the left and right sides of the pulley. If the friction coefficient of the contact surface of the cable and pulley is equal to μ and if the cable is subjected to tension force of T_1 from the left side, the tension force of the right-side cable (T_2) will be equal to $T_2 = T_1 e^{\mu\alpha}$, as shown in Fig. 5(b). In this relation, α is the contact angle of the cable with the pulley in terms of radian. According to this relation, it is considered that two parameters namely friction coefficient and contact angle between the cable and pulley increase the force on the other side of the cable. Due to the friction coefficient of 0.3 which is added to Abaqus as a fixed number, the friction force can be artificially increased by simply increasing the contact angle of the cable and pulley and in this research, at a friction coefficient value greater than 0.3, the technique of additional rotation of the cable around the pulley is used. The rise in the value of the friction coefficient in the additional rotation of the cable around the pulleys is calculated as $\mu_{eq} = \mu \times ((2n\pi + \alpha)/\alpha)$, where the parameters n and α are the number of cable rotations around the pulley and the contact angle between the cable and pulley, respectively. The increase rate of the friction coefficient in one and two additional rotations of the cable around the pulleys is calculated using Eqs. (52) and (53), respectively. It should be noted that α_0 is the contact angle of the cable and the pulley, which is defined in the analytical solution section in Eq. (6), and the value is calculated 1.08 using the shape geometry according to Eq. (51).

$$F = T_L \cos\alpha_L - T_R \cos\alpha_R \tag{50}$$

$$\alpha_0 = tan^{-1}\left(\frac{1}{d}\right) = \tan^{-1}\left(\frac{1}{\frac{b}{3h}}\right) = \tan^{-1}\left(\frac{9}{5}\right) = 1.08\ rad \tag{51}$$

$$\mu\,\alpha_0 = \mu_1\alpha_1 \rightarrow 0.3 \times (2\pi + 1.08) = \mu_1 \times 1.08 \rightarrow \mu_1 = \frac{0.3 \times (2\pi + 1.08)}{1.08} = 2.045 \tag{52}$$

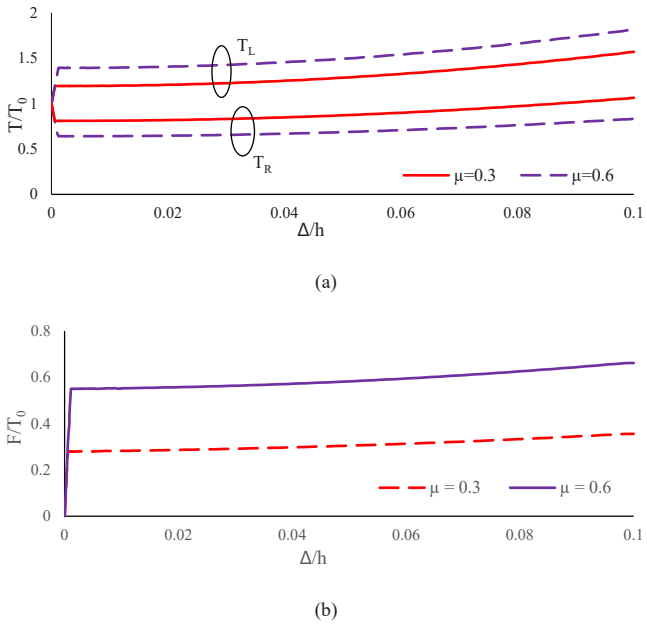

Fig. 7. (a) Normalized axial force diagram; (b) Normalized lateral resistance with friction coefficients of μ = 0.3 and μ = 0.6.

$$\mu\alpha_0 = \mu_2\alpha_2 \rightarrow 0.3 \times (4\pi + 1.08) = \mu_2 \times 1.08 \rightarrow \mu_2 = \frac{0.3 \times (4\pi + 1.08)}{1.08} = 3.79 \tag{53}$$

The diagram of the axial force and lateral resistance of the system with different friction coefficients is drawn in Fig. 6. In general, increasing the friction coefficient reduces the axial force of the right cable and increases the axial force of the left cable, lateral strength, and system stiffness, thus causing the system to remain in the static friction phase and the cable slip on the pulleys occurs later.

According to Fig. 6(a), the variation of the axial force of the cable with friction coefficients of 2.045 and 3.79 compared to the friction coefficient of 0.3 on the left side of the cable increases by 74% and 118%

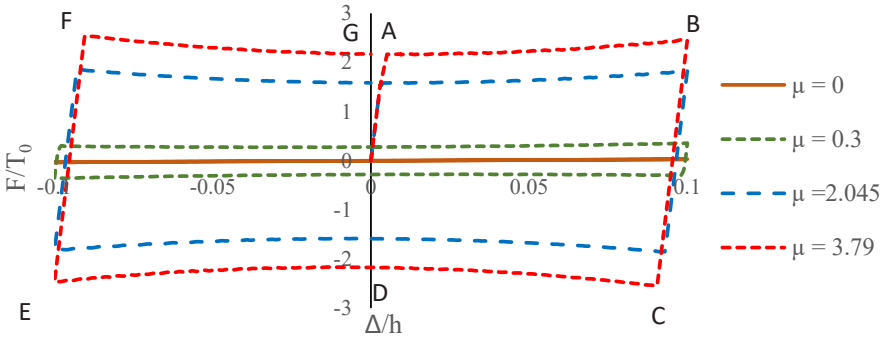

Fig. 8. System lateral resistance diagram under the effect of a cycling loading of 0.1 height in different states of friction assuming a = 5 and T_0 = 20.76 kN.

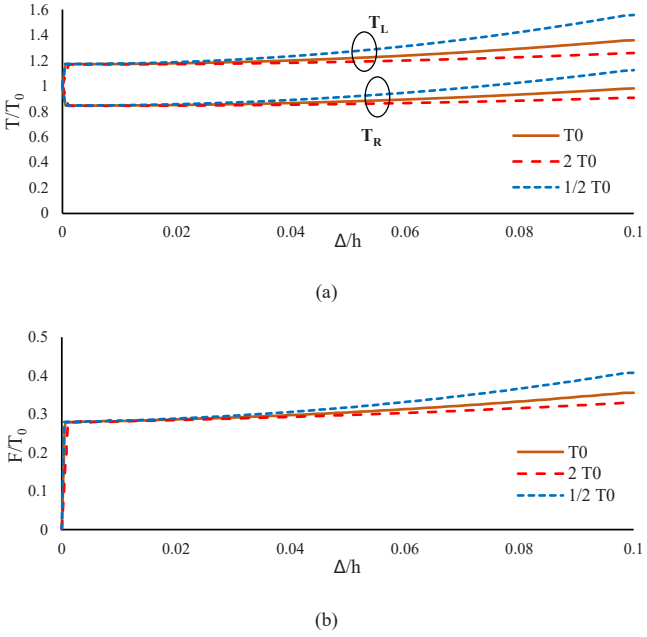

Fig. 9. (a) Normalized axial force diagram; (b) Normalized lateral resistance diagram with different pre-stressing forces by assuming a = 5 and μ = 0.3.

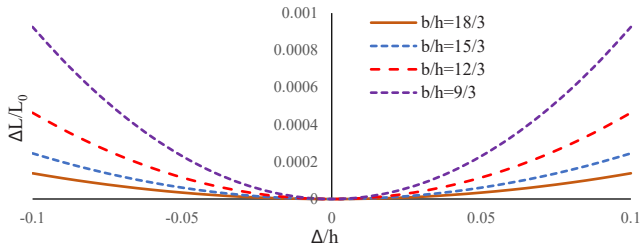

Fig. 10. Normalized cable elongation for different b/h ratios.

in the static friction phase and by 71% and 110% in the dynamic friction phase, respectively. On the right side of the cable in the static friction phase, the abovementioned variation is reduced by 74% and 84%, respectively, and also by 74% and 95%, respectively, in the dynamic friction phase.

As sketched in Fig. 3, the axial force of the left and right cables is equal in the frictionless state; therefore, the system lateral resistance has a negligible value in the nonlinear slip phase, which is obtained due to changes in the values of α_L and α_R during displacement. However, in the frictional state, the system lateral resistance is obtained from the difference in the amount of axial force of the left- and right-side cables. Similarly, it has two phases of static and dynamic frictional slip and the above results are shown in Fig. 6.

According to Fig. 6(b), the lateral resistance of the system at the friction coefficient values of 2.045 and 3.79 in the static frictional phase is 5.6 and 7.7 times the friction state of 0.3. This value in the dynamic friction phase is 5.1 and 6.8 times the friction state of 0.3. Fig. 6(c) shows the changes in the system lateral resistance with friction coefficients of 2.045 and 3.79 compared to the friction coefficient of 0.3 in two phases of the static and dynamic friction. These results are depicted from the lateral resistance diagram obtained from the finite element method (Fig. 6(b)).

Increasing the base state friction coefficient from 0.3 to 0.6 causes increase in the slope of the axial force and lateral resistance of the system, as sketched in Fig. 7. According to Fig. 7 (a), by increasing the friction coefficient from 0.3 to 0.6, the axial force of the cable on the left and right sides will increase by 20% and decrease by 20%, respectively. Moreover, according to Fig. 7(b), the system lateral resistance in the static and dynamic friction phases increases by 100% and 73%, respectively.

By increasing the friction coefficient especially when its value approaches infinity, the system lateral resistance curve converges to a single curve, and exceeding the friction coefficient from a certain range would not change the performance and lateral resistance of the system.

One of the main applications of structural systems with energy dissipation is the resistance against lateral load. This lateral load resistant systems are exposed to cyclic loading such as earthquake. Fig. 8 shows the lateral resistance diagram of the system with different friction coefficients between the cable and pulleys in a complete cyclic loading. As depicted in Fig. 8, the starting point of the figure is zero, at which there is only the pre-stressing force in the cable and the force on both sides of the right and left supports is equal, but in opposite direction. From the starting point to point A, the system lateral resistance is in the static friction phase and has a linear behavior. The slip on the cable starts from point A and enters the dynamic friction phase, which has nonlinear behavior and continues up to point B. The direction change starts from point B and there will be no slip in the range of B to C. The lateral resistance reaches zero from point B and from the point zero, the force enters the linear phase again and point C, same as point A, is the slip threshold, but starts in the opposite direction. After point C, the second slip on the cable begins to form. From point C to D, the system exhibits nonlinear behavior. The system is symmetric and in this context, the behavior of the system in the range of D to G is the same as the behavior in the range of zero to D.

The effect of the initial pre-stressing force parameter on the proposed system is investigated in three states of pre-stressing force in the base state as well as double and half the base states. By reducing the initial pre-stressing force, the stiffness of the system decreases, which leads to areduction of the system static friction phase, and the system stays less in the static friction phase before reaching the slip threshold. Fig. 9

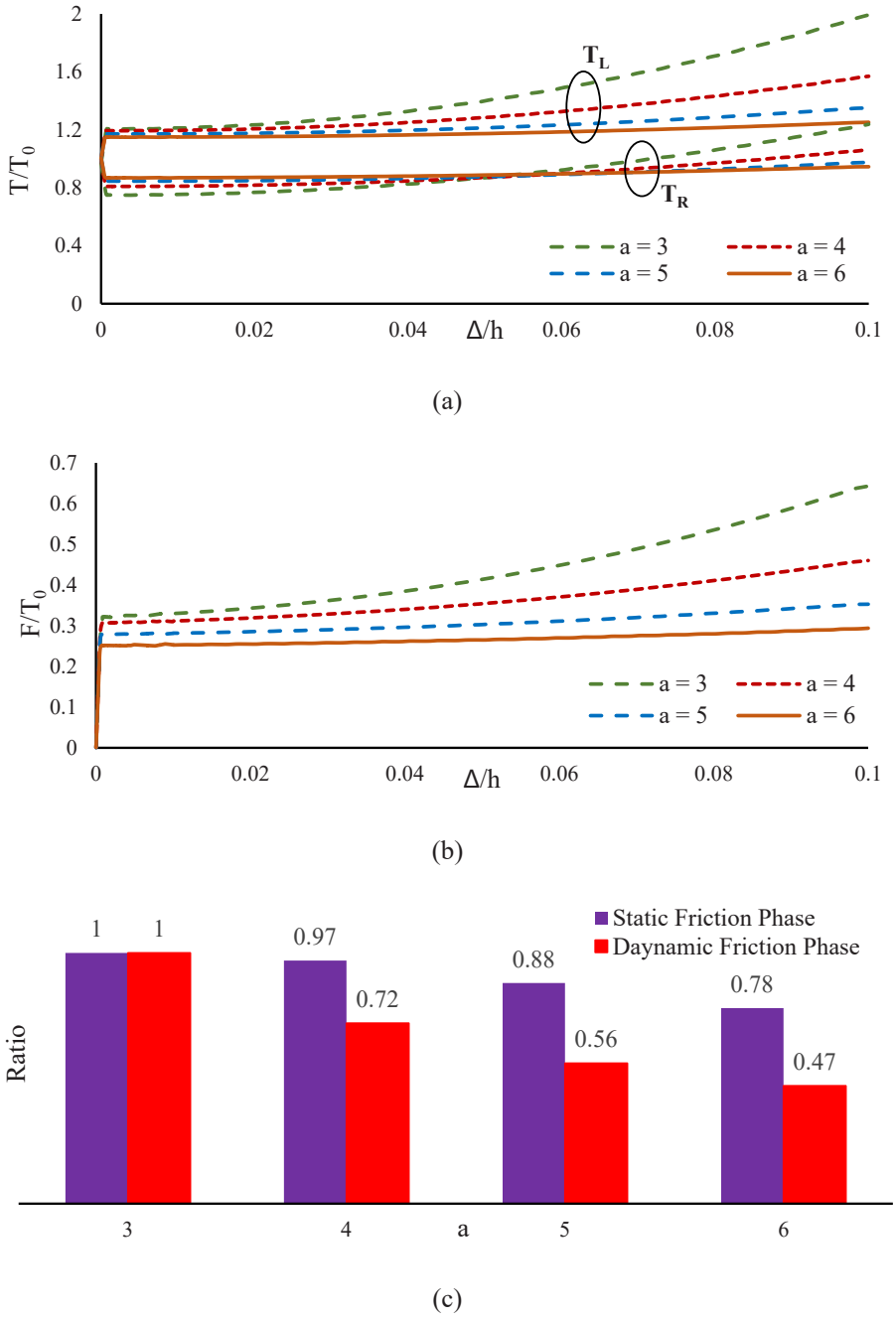

Fig. 11. (a) Normalized axial force diagram; (b) Normalized lateral resistance diagram with different span length; (c) Ratio of lateral resistance changes by assuming $T_0 = 20.76$ kN and $\mu = 0.3$.

shows the diagram of the axial force and system lateral resistance with different pre-stressing forces.

According to Fig. 9, the slip threshold of the cable axial force and the system lateral resistance for the pre-stressing force, which doubles the base state, is increased by 71% and 33%, respectively, and for the pre-stressing force that is half the base state, it is reduced by 44% and 52%, respectively, in proportion to the base state slip threshold.

Finally, the span length parameter at different spans of 3, 4, 5, and 6 m has been investigated. By changing the ratio of length to height, the strain along the cable changes and its value decreases following increase in the ratio of length to height of the cable. Moreover, the cable normalized elongation is reduced at the same lateral displacement. As a result, upon reducing the strain along the cable, the axial force of the cable is reduced, same as the lateral resistance. Fig. 10 shows the cable strain changes with the analytical solution.

As the span length increases, the contact angle between the cable and pulleys decreases, which reduces the contact surface and, thus, the effect of the friction. The effects of dimension parameter changes on the axial force and system lateral resistance are shown in Fig. 11. In general, as the span length increases, the axial force and system lateral resistance are reduced, which are also confirmed by the figures drawn through the analytical solution and Abaqus software.

According to Fig. 11(a), the span length changes with a friction coefficient of 0.3 are as follows: The axial force of the left cable for 4, 5, and 6 m spans is reduced by 0.8%, 1.5%, and 2.5% for slip threshold, respectively, and for nonlinear phase by 21%, 31%, and 36%, respectively, compared to the 3-m span. These decreasing values in the static friction phase are very small compared to those at nonlinear or dynamic

Table 1
Specifications of the steel used for the frame.

Ultimate stress	Yield stress	Density	Poisson's ratio	Young's modulus
$F_u = 370$ MPa	$F_y = 240$ MPa	$\rho = 7850\frac{kg}{m^3}$	$v = 0.3$	$E = 2.1 \times 10^5$MPa

friction phases. Furthermore, the axial force of the right cable for 4, 5, and 6 m spans for the slip threshold is reduced by 9%, 13%, and 17%, respectively, and reduced for the nonlinear phase by 15%, 21%, and 24% compared to the 3-m span. The length changes in the static friction phase on the right side of the cable are much greater than that of the left side of the cable; nevertheless, the static friction phase changes on the left side of the cable are less than those of the dynamic friction phase.

According to Fig. 11(b), the system lateral resistance reduction for 4, 5, and 6 m spans at the slip threshold is 3%, 12%, and 22%, respectively, and is 28%, 44%, and 53% in the nonlinear phase compared to the 3-m span.

Fig. 11(c) shows the lateral resistance changes for the system with different spans compared to the 3-m span in two phases of static and dynamic friction and the results are obtained from the finite element diagram (Fig. 11(b)).

5. Finite element model of moment frame and its verification and the investigation of the system cyclic behavior presented in the steel moment frame

In order to investigate the cyclic behavior of the proposed system, the considered moment frame is modeled in the Abaqus software and, then, verified by numerical reserch done by Mualla et al. [30]. For modeling, the designed frame specifications in the Taiwan international project were used by Mualla et al. Frame materials are defined as non-linear (elastic-plastic), as can be seen in Table 1. The modeled steel frame has a floor height of 3 m and a span lrngth of 5 m, and its beam and column sections are $I\,200 \times 150 \times 6 \times 9$ and $H\,200 \times 200 \times 8 \times 12$, respectively. An elasto-plastic behavior is considered for the braced frame in the case of applied displacement. The steel frame is meshed with B31 beam elements at which maximum size is 50 mm, the beam-to-column connection is rigid, and the base of columns is fixed. Furthermore, the connection between the pre-stressed cable and the column is hinged and the pulleys are prevented from rotational displacement. Fig. 12 shows the modeled moment frame without the proposed bracing system and its deformed shape. Fig. 13 shows the eccentric continuous cable bracing system implemented in the moment frame and its deformed shape.

5.1. Limitations of the structural frame system

The proposed system is investigated in a one-story, three-span frame

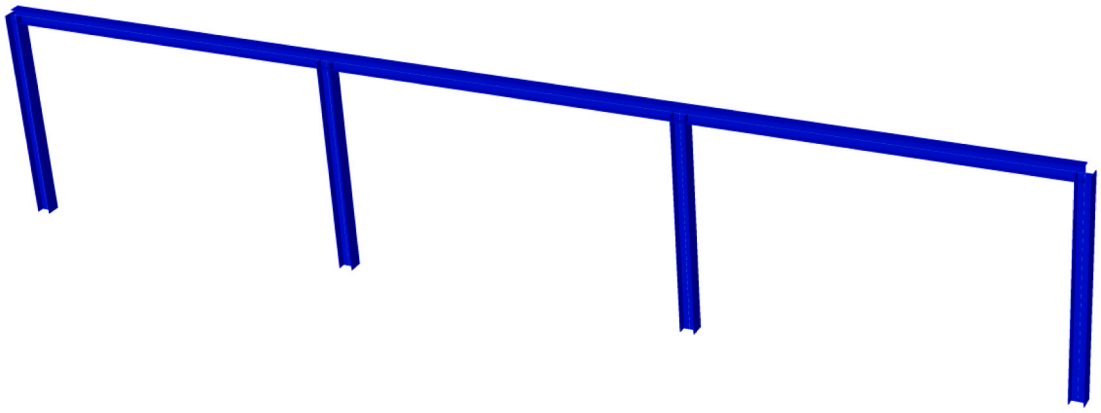

(a)

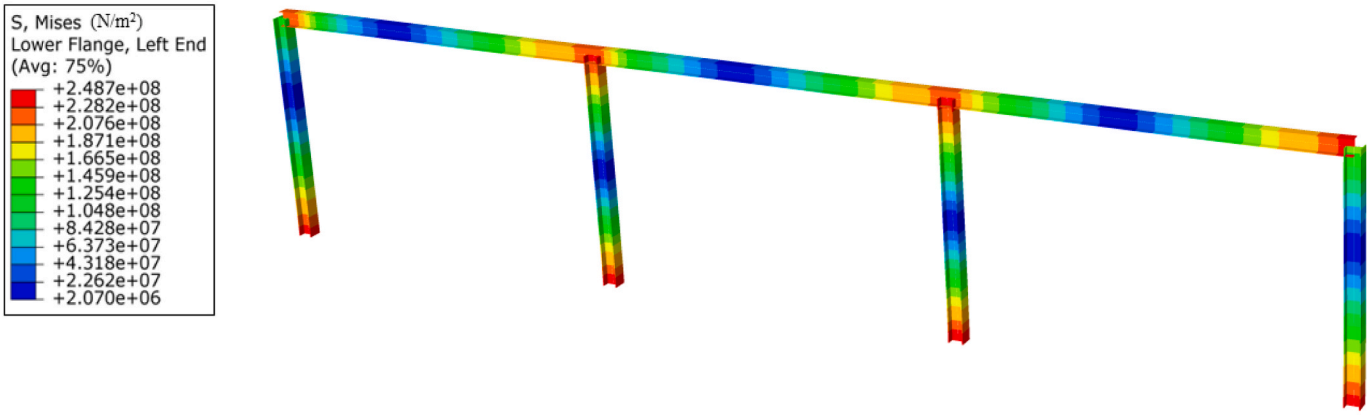

(b)

Fig. 12. (a) Modeled moment frame; (b) Deformed shape of the moment frame.

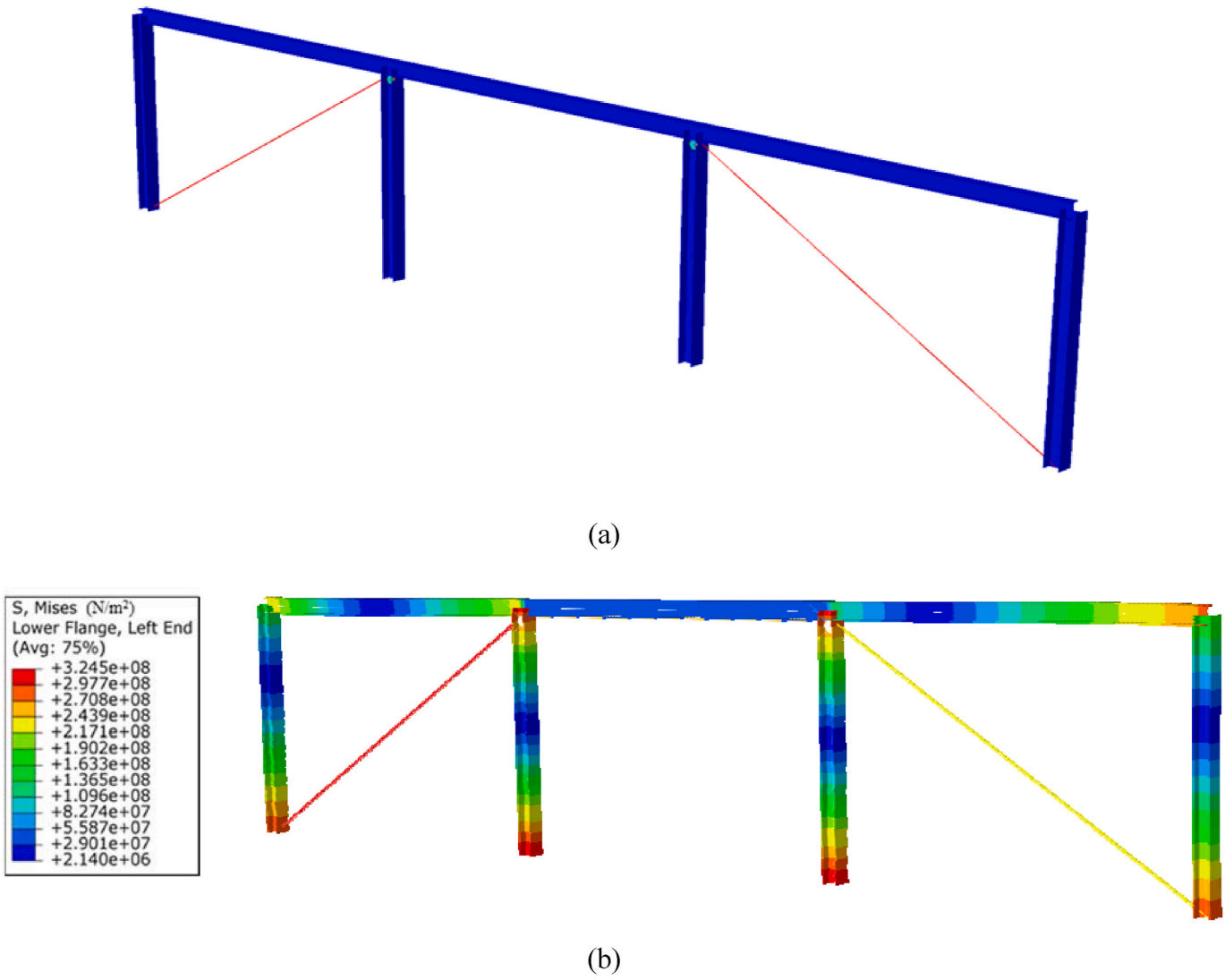

Fig. 13. (a) The eccentric continuous cable bracing system implemented in the moment frame; (b) Its deformed shape.

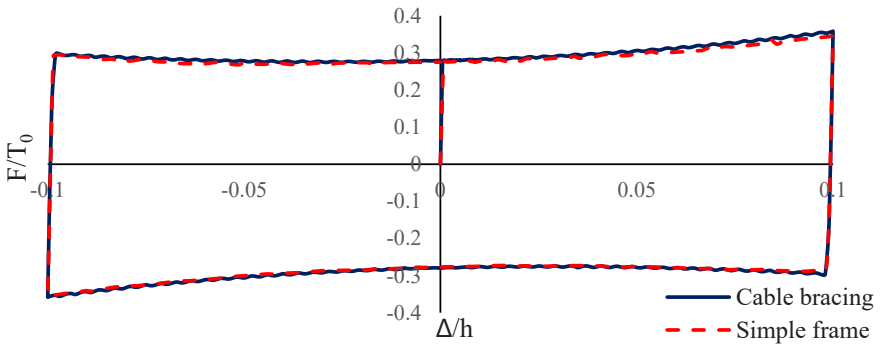

Fig. 14. Lateral resistance diagram of a simple frame with the proposed system and the proposed system under cyclic loading.

with the same span length. The frame with more stories is not investigated in this research and the proposed frame beam and column material is assumed to be the same. It has been assumed that the frame examined in this research experiences deformation only in its own plane and the displacement perpendicular to the frame nodes plane is ignored. It is also assumed that there is sufficient lateral stiffness and restraint in the direction perpendicular to the frame plane. In addition to the mentioned limitations, the pulleys are restricted from rotational displacement inside the column and there is no relative displacement for the pulley with respect to the top of the corresponding column. Each pulley experiences the same displacement as that of the top of column.

5.2. Verification of the hinged frame with the cable and pulley bracing system

To verify the frame with the cable and pulley bracing system, the

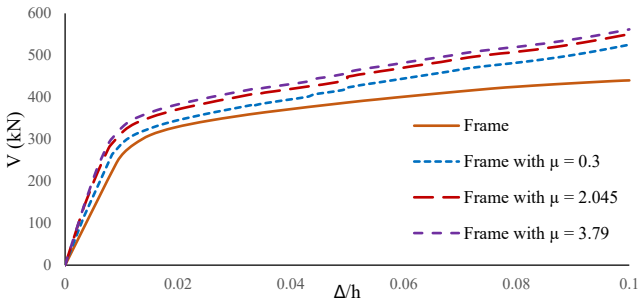

Fig. 15. Pushover diagram of a steel moment frame and a steel moment frame with the proposed system involving different friction coefficients.

connections and frame supports are considered hinged. Moreover, the friction between cable and pulleys is considered 0.3. In this case, the frame shows almost no structural resistance against lateral loads and plays the role of supporting the proposed cable bracing system. In this condition, the diagram of the shear force transferred to the support by the cable under cyclic loading should be equal to the lateral resistance diagram of the proposed cable bracing system without a frame under cyclic loading. The above result is shown in Fig. 14.

Fig. 15 shows the pushover analysis of the moment frame and the moment frame with the proposed cable bracing in different states of friction and accordingly, by adding the cable bracing system to the frame, the initial stiffness of the whole system (frame with cable and pulleys system) increases compared to the frame without cable bracing system, and the static friction phase and the cable slip on the pulleys occur sooner.

5.3. Investigation of the proposed system cyclic behavior in steel moment frame

During an earthquake, the structure loading will be cyclic based on the nature of this load. For this reason, it is not acceptable to use monotonic loading to investigate the non-linear behavior of the structure and its elements, because the important parameters of stiffness reduction and strength degradation in ductility are not included. To this end, for investigating the hysteresis behavior of the frame system with cable and pulleys, ATC24 loading protocol was used in the connection between the beam and the column. The entered cyclic loading to the system is depicted in Fig. 16, which has a displacement range of 0.1 m. The base shear force diagram in the moment frame and the frame with cable and pulley bracing system models with a friction coefficient of 0.3 under cyclic loading is drawn in Fig. 17. As shown in the figure, by applying the proposed bracing system to the structural frame, the shear force transmitted to the base increases and the dissipated energy increases. The area under the hysteresis diagram or, in other words, the area inside the hysteresis diagram, represents the dissipated energy. This dissipated energy is obtained by both calculating the area inside the hysteresis diagram by interface software and Abaqus software. Fig. 18 shows the diagram of the cumulative dissipated energy of the moment frame and the moment frame with the proposed bracing system. According to Fig. 18 and the calculation of area inside the hysteresis loops in Fig. 17 in the moment frame without braces, the dissipated energy is 520 kJ. In this case, the dissipated energy results from the formation of plastic hinges in the beam; however, with the addition of an eccentric continuous cable bracing system with a friction coefficient of 0.3 to the moment frame, the amount of energy dissipation is increased by 19%–620 kJ. Therefore, this state of friction between the cable and the pulleys leads to energy dissipation.

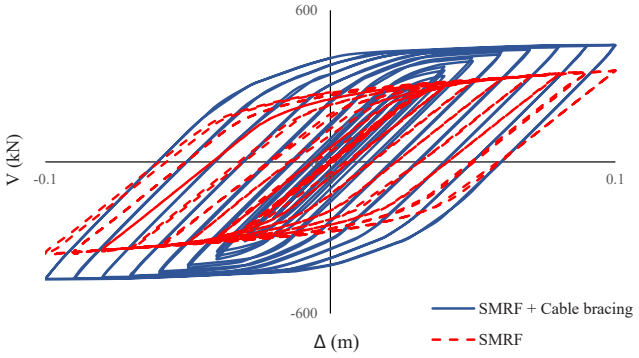

Fig. 17. Hysteresis diagram of the steel moment frame and the steel moment frame equipped by the proposed cable system with a friction coefficient of 0.3.

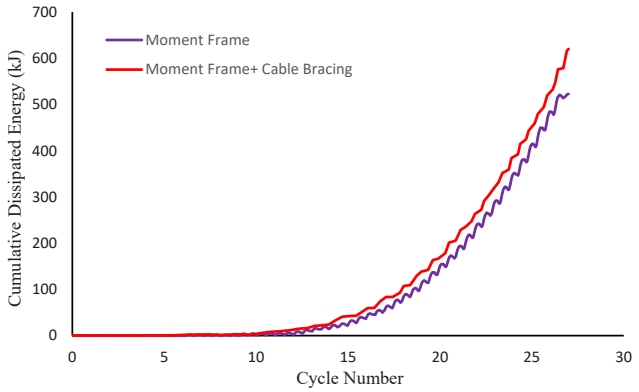

Fig. 18. Cumulative dissipated energy diagram of the moment frame and the moment frame with the proposed cable bracing and pulley system.

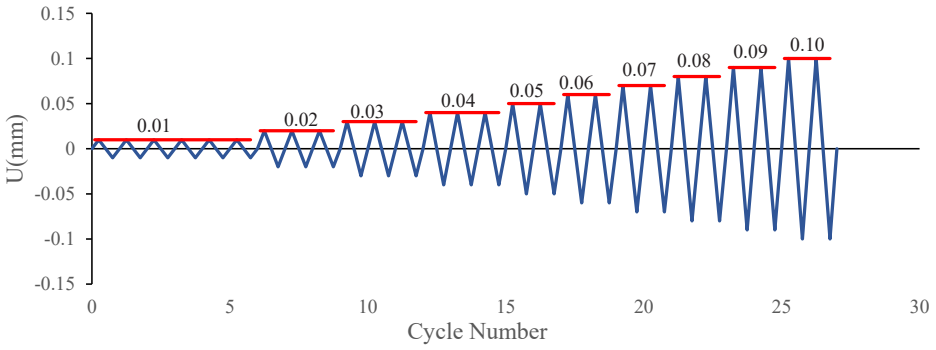

Fig. 16. ATC24 loading protocol.

6. Conclusion

In this research, a cable bracing system consisting of a pre-stressed cable passing over fixed pulleys was proposed to provide stiffness and lateral resistance in structural frames. In addition to providing lateral strength for the structure, the proposed system also provided energy dissipation through frictional slipping between cable and pulleys. The proposed system had a two-phase resistant behavior in which the first phase was linear elastic with high stiffness while the second phase was nonlinear, increasing stiffness with input energy dissipation. The mentioned result was obtained by two methods of analytical solution and finite element model. Moreover, the most important parameters affecting the system were studied and at the end, the behavior of the moment frame with the proposed bracing system was investigated. The most important research results were as follows:

1) The proposed system, in addition to the lateral restraint of the structure, has the capacity to dissipate the input energy.
2) In the proposed system, the whole cable is always in tension and loosening does not occur.
3) The two-phase behavior of the system is one of its main characteristics; thus, the system has a linear behavior with high stiffness in case of a small displacement such as the usual wind force and in the case of a large displacement such as a severe earthquake, the system experiences nonlinear phase and exhibits a nonlinear behavior with increasing stiffness, which prevents the growing displacement of the system.
4) The resistant behavior of the system and its energy dissipation capacity can be investigated and adjusted by three main parameters of friction coefficient, initial pre-stressing force, and span length.
5) To check the effect of friction coefficient parameter, additional rotation of the cable around the pulleys is considered and further increase of friction effect is calculated using the friction coefficient formula equivalent to $\mu_{eq} = \mu \times ((2n\pi + \alpha)/\alpha)$.
6) Increasing the friction coefficient leads to the reduction of the axial force of the right side of the cable, thus the axial force of the left side of the cable increases and the lateral resistance and initial stiffness of system rises. As a result, stiffness increase leads to an increase in range of static friction phase and the pulleys slipping over the cable occurs later.
7) The axial force of the cable with friction coefficients of 2.045 and 3.79 compared to the friction coefficient of 0.3 on the left side of the cable is increased by 74% and 118% in the static friction phase and by 71% and 110% in the dynamic friction phase, respectively. In addition, on the right side of the cable in the static friction phase, it is reduced by 74% and 84%, respectively, and by 74% and 95% in the dynamic friction phase.
8) Increasing the base state friction coefficient from 0.3 to 0.6 leads to an increase in the system lateral resistance and the amount of the increase in the static and dynamic friction phases is 100% and 73%, respectively.
9) High values of the friction coefficient do not lead to any changes in the structure performance and the lateral resistance curve of the system converges to a single curve.
10) Reducing the initial pre-stressing force reduces the initial stiffness of the system, thus leads to a reduction in the static friction phase and the system displacement until the slip threshold is reached.
11) By increasing the ratio of the cable length to its height, the system strain decreases and leads to reduction of the axial force of the system.
12) Upon increase in the span length, the system lateral resistance decreases. With increase in the span length from 3 to 5 m, the lateral resistance of the system in the static and dynamic friction phases is reduced by 12% and 44%, respectively.
13) Addition of the cable bracing system to the moment frame increases the system stiffness in the static friction phase and the cable slipping on the pulleys occurs later. In addition, its energy dissipation increases by 19% compared to the frame without bracing.

Authorship statement form

*The authors are individuals who satisfy **ALL** of the following conditions:*

1) contribute to the conception and design, acquisition of data, or analysis and interpretation of data;
2) drafted the manuscript or revised it critically for important intellectual content
3) finally approved the version to be published. Each author is responsible for the appropriate fragments of the manuscript, its content and for potential conflicts of interest. Persons who do not meet the above criteria should be listed (with prior written consent) in the acknowledgments.

The undersigned hereby declare that:

1. the manuscript is original, does not infringe any copyright or other proprietary rights of third parties, is not submitted for publication to another journal, and has not been previously published;
2. upon publication the undersigned author(s) transfer(s) all copyright ownership of the aforementioned manuscript to the journal Annals of Parasitology;
3. contribution of individual authors to manuscript preparation is defined in terms of the following criteria:

a. Investigation;
b. Software;
c. Writing draft;
d. Original draft;
e. Conceptualization;
f. Methodology;
g. Supervision;
h. Validation;
i. Data curation;
j. Visualization;
k. Writing reviewing and editing;

Declaration of competing interest

The authors declare that they have no known competing financial interests or personal relationships that could have appeared to influence the work reported in this paper.

Data availability

Data will be made available on request.

References

[1] Partovi F, Fanaie N. Controlling deflection of long steel I-shaped girder bridge using two V-shaped pre-tensioning cable. J Cent Sout Univ Technol 2020;27(2):566–77.
[2] Hou X, Tagawa H. Wire-rope bracing system with elasto-plastic dampers for seismic response reduction of steel frames. In: The 14th world conference on earthquake engineering; 2008. p. 12–7.
[3] Hou X, Tagawa H. Displacement-restraint bracing for seismic retrofit of steel moment frames. J Constr Steel Res 2009;65:1096–104.
[4] Fanaie N, Aghajani S, Afsar Dizaj E. Strengthening of moment-resisting frame using cable–cylinder bracing. Adv Struct Eng 2016;19(11):1736–54.
[5] Fanaie N, Aghajani S, Dizaj EA. Theoretical assessment of the behavior of cable bracing system with central steel cylinder. Adv Struct Eng 2016;19(3):463–72.

[6] Fanaie N, Aghajani S. Wire-rope bracing system with central cylinder, element based application finite element based application. In: Proceedings of the 15th earthquake engineering conference; 2012.
[7] Fanaie N, Zafari N. Seismic study of cable-cylinder bracing under near field records. In: Proceeding of the 7th National and 2nd International conference steel and structure; 2017.
[8] Fanaie N, Zafari N. Sensitivity analysis on response modification factor of new cable-cylinder bracing systems. J Earthq Eng 2019;23(4):648–68.
[9] Zahrai SM, Mousavi SA. Cable-pulley brace to improve story drift distribution of MRFs with large openings. Steel Compos Struct 2016;21(4):863–82.
[10] Mehrabi M, Ibrahim Z, Ghodsi S, Suhtril M. Seismic characteristics of X-cable braced frames bundled with a pre-compressed spring. Soil Dynam Earthq Eng 2019;116:732–46.
[11] Nishimura I. Performance evaluation of damping devices installed in a building structure. J Struct Constr Eng–Trans Arch Inst Jpn 2004;579:23–30.
[12] Symans MD, Charney FA, Whittaker AS, Constantinou MC, Kircher CA, Johnson MW, McNamara RJ. A Energy dissipation systems for seismic applications: current practice and recent developments. J Struct Eng 2008;134(1):3–21.
[13] Lavan O, Dargush GF. Multi-objective evolutionary seismic design with passive energy dissipation systems. J Earthq Eng 2009;13(6):758–90.
[14] De Domenico D, Hajirasouliha I. Multi-level performance-based design optimisation of steel frames with nonlinear viscous dampers. Bull Earthq Eng 2021; 19(12):5015–49.
[15] Nishimura I. Performance evaluation of a building structure with nonlinear dampers under strong ground motion on March 11. In: 14th US-Japan workshop on improvement of structural design and construction practices; 2012; 2011.
[16] Montuori R, Nastri E, Pluso V. The use of TPMC for designing MRFs equipped with FREEDAM connections: performance evaluation. Key Eng Mater 2018:983–91.
[17] Latour M, Piluso V, Rizzano G. Free from damage beam-to-column joints: testing and design of DST connections with friction pads. Eng Struct 2015;85:219–33.
[18] Monir HS, Zeynali K. A modified friction damper for diagonal bracing of structures. J Constr Steel Res 2013;87:17–30.
[19] Pall AS. Limited slip bolted joints: a device to control the seismic response of large panel structures. Concordia University; 1979.
[20] Quintana HC, Petkovski M. Optimum performance of structural control with friction dampers. Eng Struct 2018;172:154–62.
[21] Pall AS, Marsh C. Response of friction damped braced frames. J Struct Div 1982; 108(6):1313–23.
[22] Chien CSC, Lu LY, Tsai YL. Analysis of single-degree-of-freedom systems containing multi-functional friction damper. Procedia Eng 2014;79:500–5.
[23] Chacar JPM. Design of cable systems for cable suspension bridges. Massachusetts Institute of Technology; 2011.
[24] Moghaddam H, Afzalinia F, Hajirasouliha I. Optimal distribution of friction dampers to improve the seismic performance of steel moment resisting frames. Structure 2022;37:624–44.
[25] Vezina S, Proulx P, Pall R, Pall A. Friction-dampers for aseismic design of Canadian space agency. In: 10th World conference on earthquake engineering; 1992. p. 4123–8.
[26] Mualla IH, Belev B. Performance of steel frames with a new friction damper device under earthquake excitation. Eng Struct 2002;24:365–71.
[27] Bagheri S, Shishvan SS, Barghian M, Baniahmad B. A new energy dissipative cable bracing system. Adv Struct Eng 2019;22(14):3134–46.
[28] Hernandez H, Astroza R, Beltran JF, Zhang X, Mercado V. A experimental Study of a cable-pulleys spring-damper energy dissipation system for buildings. J Build Eng 2022.
[29] Hibbitt H, Karlsson B, Sorensen P. ABAQUS-6.12-1. 2012. Standard user's manual.
[30] Mualla I, Nielsen L, Belev B, Liao W, Loh C, Agrawal A. Numerical predictions of shaking table tests on a full scale friction-damped structure. In: 12th European conference on earthquake engineering, London, UK; 2002.